Fourier conjugate adaptive optics for deep-tissue large field of view imaging

Amitonova, Lyubov V.

published in
Applied Optics
2018

DOI (link to publisher)
10.1364/AO.57.009803

document version
Publisher's PDF, also known as Version of record

citation for published version (APA)
Amitonova, L. V. (2018). Fourier conjugate adaptive optics for deep-tissue large field of view imaging. *Applied Optics*, *57*(33), 9803-9808. https://doi.org/10.1364/AO.57.009803

Research Article Vol. 57, No. 33 / 20 November 2018 / Applied Optics 9803

applied optics

Fourier conjugate adaptive optics for deep-tissue large field of view imaging

Lyubov V. Amitonova[1,2]

[1]Biomedical Photonic Imaging Group, University of Twente, P.O. Box 217, 7500 AE Enschede, The Netherlands
[2]LaserLaB, Department of Physics and Astronomy, Vrije Universiteit Amsterdam, De Boelelaan 1081, 1081 HV Amsterdam, The Netherlands (l.amitonova@vu.nl)

Received 17 August 2018; revised 25 October 2018; accepted 26 October 2018; posted 29 October 2018 (Doc. ID 342570); published 19 November 2018

Light microscopy enables multifunctional imaging of biological specimens at unprecedented depths and resolutions. However, the performance of all optical methods degrades with the imaging depth due to sample-induced aberrations. Methods of adaptive optics (AO), which are aimed at pre-compensation of these distortions, still suffer from a limited field of view and imaging depth as well as inconvenient microscope design. Here, I propose and investigate a new approach to overcome these limitations: Fourier image plane conjugate AO. Two experimental designs of the new approach are carefully studied, and an accurate comparison between different methods of AO is presented. Fourier conjugate AO provides a larger field of view, which can only be limited by the angular memory effect, and allows the optimal use of the spatial light modulator. Moreover, theoretically possible imaging depth of Fourier conjugate AO is limited only by the working distance of the objective and not by the microscope design.

https://doi.org/10.1364/AO.57.009803

1. INTRODUCTION

Light microscopy has been a key tool for biological and medical research for centuries [1]. Optical approaches can provide high spatial resolution, together with extended functionality produced by the number of different contrast mechanisms [2,3]. However, light scattering in biological tissues restricts *in vivo* application of these techniques to the near-surface region [4].

Nowadays, the most popular strategy to overcome this limit is to use only ballistic photons. Methods of fluorescent microscopy such as confocal microscopy and nonlinear microscopy exploit this scenario. Unfortunately, the number of ballistic photons decays exponentially with depth (following the Beer–Lambert law) leading to an enormous drop in the signal after several mean free paths of a photon [4]. As a result, the imaging depths of fluorescent nonlinear microscopy techniques are still limited to approximately 1 mm even in state-of-the-art works [5,6]. Currently, only invasive fiber probes can be used for high-resolution deep-tissue optical imaging [7,8].

The next breakthrough on the way to noninvasive deep-tissue *in vivo* optical microscopy is the implementation of an advanced adaptive optics (AO) technique [9]. The typical AO technique addresses only the aberrations problem and works in the regime where the aberrations are smooth functions of the spatial coordinates. Until recently, these methods were considered impractical for thick multiple scattering samples with high losses of ballistic photons due to light scattering [10,11]. This concept changed after the work of Vellekoop and Mosk [12], which demonstrated the wavefront-shaping technique. Active wavefront shaping allows the creation of diffraction-limited focus behind the highly scattering sample in the diffusive light propagation regime [13,14]. Nowadays, we can address the power loss due to scattering and utilize scattered photons for imaging by using wavefront shaping.

Methods of adaptive optics in combination with nonlinear fluorescent microscopy, such as two-photon microscopy, are considered to be promising for deep-tissue imaging [15–17]. The concept of wavefront manipulation in the multiple scattering regime is a pervasive concept, with the potential to open new horizons in deep-tissue noninvasive microscopy [9].

The most common AO approach involves placing a deformable mirror or spatial light modulator (SLM) in the pupil plane of the imaging device, which is a standard telescope in $4f$ configuration [18]. However, such a design is appropriate only in the case when the aberrations to be compensated are spatially invariant. Otherwise, it imposes a severe limitation on the field of view (FOV) [19].

More promising is the conjugate adaptive optics configuration, which includes placing the spatial light modulator conjugate to the main source of aberrations. It allows the utilization of the angular memory effect [20,21]. The angular optical memory effect predicts that tilting the incident beam over small angles does not change the resulting speckle pattern but only

translates it. As a result, conjugate AO allows the use of part of the previously optimized wavefront during the scanning procedure and provides a significant FOV advantage [22,23]. The efficiency of this approach was demonstrated in recent experiments [16,24–27].

Conjugate AO is a powerful method, which allows high-resolution *in vivo* imaging of a mouse brain through the intact skull [28]. However, the field of view is still quite limited, and, despite all potential advantages for deep-tissue microscopy, the imaging depth typically does not exceed 1 mm. On top of this, to place the SLM in the conjugate plane in the focusing beam is an experimental challenge, especially for high imaging depths [22].

Here, I propose and investigate a more powerful method of adaptive optics: Fourier image plane conjugate AO. The proposed method retains all advantages of conjugate AO microscopy while providing further improvements, which are especially crucial for deep-tissue imaging: (1) it provides high FOV within the memory effect range even if pre-compensation was done only for a single point; (2) it provides imaging depth theoretically limited only by working distance of the objective and not by the microscope design; and (3) it does not require putting the SLM in the focusing beam. As a result, it simplifies microscope design and excludes possible thermal damage of the SLM due to high-powered lasers, which are widely used for deep-tissue nonlinear microscopy. Moreover, it allows the optimal use of SLM resolution, which is critical in the case of wavefront shaping in highly scattering samples. The quality of the focal spot behind the scattering media can be characterized by enhancement, which is defined as a ratio between the intensity in the target after optimization and the ensemble averaged transmitted intensity before optimization. Enhancement is proportional to the number of segments used for wavefront shaping [29]. It means that it is crucial to use the full resolution of the SLM.

2. ANALYTICAL MODEL

All approaches were analytically characterized by using the thin lens equation in the paraxial ray approximation in terms of the best possible FOV, imaging depths, and optimal microscope parameters.

The fundamental concepts of optical setups suitable for different techniques of conjugate adaptive optics are presented in Fig. 1. For simplicity, lenses L_1, L_2, and L_3 have the same focal distances, and the system has unit magnification. Dotted green lines represent the pupil planes, and dashed black lines represent the imaging planes. Blue arrows indicate elements that should be moved for scanning in depth. Single-plane phase distortion (single scattering layer) is shown by the black curved line after lens L_3. The SLM position is shown by the blue line.

A thin scattering layer was chosen as a vivid example for explanation of the conjugate adaptive optics techniques. However, the experimental design allowing imaging of a sample with a single scattering layer is not entirely artificial. It was shown recently that a single conjugated wavefront correction might substantially increase the corrected field of view in some relevant biological systems, such as the brain, which is covered by a single dominant scattering layer, i.e., the skull [28].

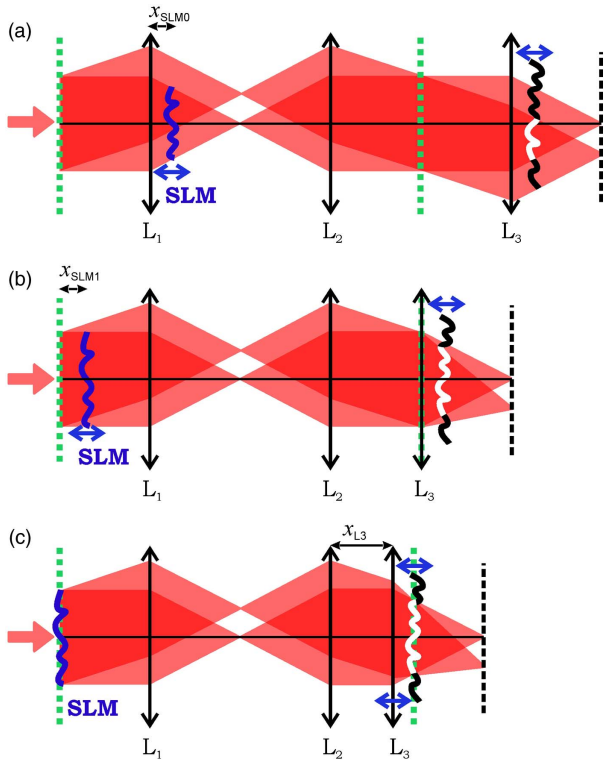

Fig. 1. Illustration of the main ideas of different conjugate AO methods for nonlinear microscopy. (a) Standard conjugate AO. (b), (c) Two designs of proposed Fourier conjugate AO. Lenses L_1, L_2, and L_3 have the same focal distances. Dotted green lines represent the pupil planes. Dashed black lines represent the imaging planes. Blue arrows indicate movable elements. Single-plane phase distortion is shown by the black curved line after lens L_3. The SLM position is shown by the blue line. The distortion is fully pre-compensated for zero angle. For nonzero angles, the pre-compensation works only partially—the white part of the black curved line after lens L_3. We already see that, for the same parameters of the optical system and the same input angles, pre-compensation works better in the case of Fourier conjugate AO.

Here, we consider adaptive optics for nonlinear microscopy applications. We assume that pre-compensation can be performed only for a single scan angle. Calibration with a few guide stars at different locations (several scan angles) is not possible for highly scattering biological sample in a noninvasive way. Noninvasive optical wavefront shaping in a diffuse regime can be only done by using total nonlinear fluorescent feedback, as shown recently [30]. Total nonlinear feedback wavefront shaping creates a single focus, and its lateral location is not controlled or predetermined. As a result, the distortion is fully pre-compensated for a single input angle. For other input angles, the pre-compensation works only partially—the white part of the black curved line after lens L_3. Here, we assume an infinite memory effect range.

The main principle of a typical optical setup for standard conjugate AO technique is presented in Fig. 1(a), where the SLM is placed in the plane where the image of a scattering layer with a lens system $\{L_2\ L_3\}$ is formed. The single scattering layer is represented by a solid black curve. The optimal wavefront for

the zero angle is projected on the SLM, as shown in Fig. 1(a) by the solid blue curve.

The illustration of the main principle of Fourier conjugate AO is presented in Figs. 1(b) and 1(c). The spatial light modulator is placed in the plane where the image of the scattering layer with the lens system {L_1 L_2 L_3} is formed, the so-called Fourier image plane. This new approach allows for the realization of different microscope designs.

In the first design, lens L_3 is fixed and placed into the focal plane of lens L_2 [see Fig. 1(b)]. The optimal wavefront for the zero angle is projected on the SLM, and the aberration is partially compensated (white part of the distorted phase), depending on the scan angle. We can easily see that the proposed approach allows more efficient usage of an angular optical memory effect. The compensated area in Fourier conjugate AO is much higher than in standard conjugate AO for the same parameters of optics and scan angles [compare solid white curves in Figs. 1(a) and 1(b)].

In the second design of Fourier conjugate AO, lens L_3 is placed in such a way that a "pupil" plane at the position of the scattering layer is formed. The SLM is placed into the back focal plane of lens L_1, and its position is fixed [see Fig. 1(c)]. For proper conjugation, the position of lens L_3 should be adjusted. We see that this design allows us to maintain full compensation of the aberrations independent of the scan angle [beam is always within a pre-compensation area; white curve in Fig. 1(c)]. Resultantly, in this microscope configuration, FOV is limited only by an angular memory effect range, which is infinite for a single scattering layer.

First, we analyze the difference in FOV for standard conjugate AO and Fourier conjugate AO in the case of a single scattering layer and single focus pre-compensation. Here, potential FOV is estimated as a distance at which focusing is done with half of the wavefront along this axis fully compensated. We can see that, for standard conjugate adaptive optics (CAO), FOV is given by $\mathrm{FOV}_{\mathrm{CAO}} \propto D \cdot f_2 \cdot l/(f_1 \cdot f_3)$; for the first configuration of Fourier conjugate adaptive optics (FCAO) by $\mathrm{FOV}_{\mathrm{FCAO}} \propto D \cdot f_2 \cdot l/(f_1 \cdot (f_3 - l))$, where f_1, f_2, and f_3 are focal lengths of L_1, L_2, and L_3 lenses, respectively, l is the distance between the scattering layer and the focal plane [imaging depth beyond the scattering layer; see Figs. 1(a) and 1(b)], and D is the input beam diameter.

The ratio between $\mathrm{FOV}_{\mathrm{FCAO}}$ and $\mathrm{FOV}_{\mathrm{CAO}}$ as a function of normalized imaging depth beyond the scattering layer, l/f_3, is plotted in Fig. 2(a). We see the significant enhancement of FOV in Fourier conjugate AO, especially for large imaging depths. Moreover, the second configuration of Fourier conjugate AO, which is presented in Fig. 1(c), provides imaging with FOV limited only by the angular optical memory effect.

Second, we calculate the optimal positions of the SLM for the setups presented in Figs. 1(a) and 1(b) and optimal position of the L_3 lens for the setup presented in Fig. 1(c). The position of the SLM for the standard conjugate AO [setup presented in Fig. 1(a)] is given by $x_{\mathrm{SLM0}} = f_1 - l \cdot (f_2/f_3)^2$; the position of the SLM for Fourier conjugate AO in the first configuration [setup presented in Fig. 1(b)] is given by $x_{\mathrm{SLM1}} = f_3 \cdot (f_1/f_2)^2 (f_3/l - 1)$; the position of lens L_3 for Fourier conjugate AO in the second configuration [setup presented in Fig. 1(c)] is given by $x_{\mathrm{L3}} = f_2 - f_3(f_3/l - 1)$.

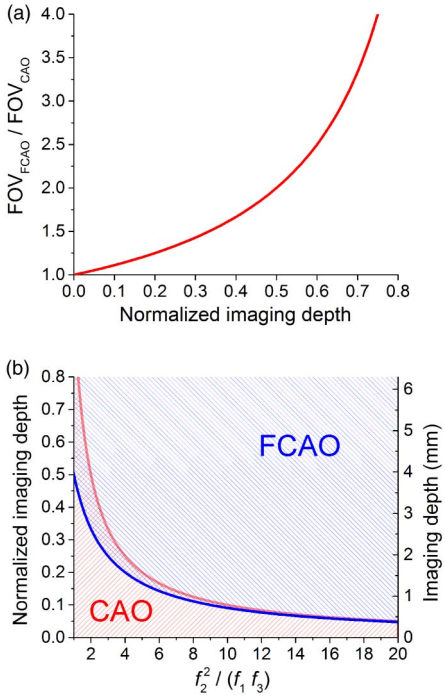

Fig. 2. (a) FOV advantage of Fourier conjugate AO. The ratio between FOV in Fourier conjugate AO (FCAO) and FOV in standard conjugate AO (CAO), as a function of normalized imaging depth beyond the scattering layer l/f_3. (b) Limits of possible normalized imaging depth beyond the scattering layer, l/f_3, as a function of p parameter of the optical system, $p = f_2^2/(f_1 f_3)$, for standard conjugate AO (red line) and Fourier conjugate AO (blue line). Possible imaging depths are situated below the red curve for standard conjugate AO (red dashed area) and above the blue curve for Fourier conjugate AO (blue dashed area). The right axis shows the imaging depth in mm for typical microscope objective with $f_3 = 9$ mm. Limit for the second configuration of Fourier conjugate AO is equal to the limit of the first configuration for the case of $f_1 = f_2$.

By using these data, we can characterize the flexibility of the microscope configurations and find the imaging depth limits for all microscope setups. As a result, $l/f_3 < 1/p$ for standard conjugate AO, $l/f_3 > 1/(p+1)$ for the first configuration [see Fig. 1(b)], and $l/f_3 > 1/(f_2/f_3 + 1)$ for the second configuration [see Fig. 1(c)] of Fourier conjugate AO, where $p = f_2^2/(f_1 f_3)$ is a normalized parameter of an optical system.

The results are presented in Fig. 2(b), where the limitations of normalized imaging depths beyond the scattering layer, l/f_3, are plotted as functions of the p parameter of a system for different adaptive optics techniques. The red line corresponds to the upper limit for standard conjugate AO, and the blue line represents a lower limit for the first configuration of Fourier conjugate AO. Theoretically possible imaging depths lie below the red curve for standard conjugate AO [red dashed area in Fig. 2(b)] and above the blue curve for Fourier conjugate AO [blue dashed area in Fig. 2(b)]. The limit for the second configuration of Fourier conjugate AO is equal to the limit of the first configuration for the case of $f_1 = f_2$.

We see that the two methods of conjugate AO suffer from different limitations. Standard conjugate AO always works for small imaging depths, but, for increasing imaging depth, we need to move the SLM closer to lens L_1, thereby placing a theoretical limit on the parameters of the optical system and reachable imaging depths. In contrast, Fourier conjugate AO always works for large imaging depth, with the limit arising as imaging depth is lowered. For decreasing imaging depth, we need to move the SLM closer to lens L_1 in the first Fourier conjugate AO configuration and move lens L_3 closer to lens L_2 in the second Fourier conjugate AO configuration.

Despite the fact that both approaches have parameters, which allow us to use the full depth range, Fourier conjugate AO is more appropriate for deep tissue imaging. Microscopy setups based on conjugate AO require a decrease in focal distance of lens L_1 to increase imaging depth. For example, standard conjugate AO microscopes optimized for typical objectives with large working distances, such as UMPLFLN Olympus (20×, NA = 0.5; WD = 3.5 mm) and LMPLFLN Olympus (20×, NA = 0.4; WD = 8 mm), provide a maximal imaging depth of only 1.8 and 2 mm, respectively. In calculations, we take the minimal focal length of lens L_1 as 50 mm, SLM size of 10 mm, and input beam diameter of 10 mm.

In contrast, Fourier conjugate AO approaches [see Figs. 1(b) and 1(c)] provide imaging depth limited only by working distance of the objective. As a result, if we aim at deep-tissue imaging, it is preferable to use the proposed method of Fourier conjugate adaptive optics.

The final advantage of Fourier conjugate AO is related to practical reasons of convenience and stability of an experimental setup as well as optimal usage of SLM pixels. In standard conjugate AO approaches, the SLM is placed into the focusing beam [22]. It means that, for different imaging depths, a different number of pixels for phase compensation is available. It will greatly influence the quality of wavefront pre-compensations for different depths. For Fourier conjugate AO, the beam on the SLM is always parallel, and a number of pixels used does not depend on imaging depth. It also excludes possible thermal damage of the SLM. Moreover, the second configuration of Fourier conjugate AO setup fixes the SLM position for different imaging depths. This makes Fourier conjugate AO more suitable for 3D visualization.

3. NUMERICAL SIMULATIONS

Numerical simulations of beam propagations are made to confirm theoretical predictions. A beam propagation method in the frequency domain is used for the numerical solution of the Helmholtz equation in free space. Field propagation through the microscope is taken to be through free space, except for the presence of a thin aberrating layer located at distance l from the object and simulated as a thin phase screen of transmission. An artificially generated random phase mask presented in Fig. 3(e) is used. The SLM is also simulated as a thin phase screen of transmission at the appropriate position. On the virtual SLM, only the central part of the phase is projected, as if someone characterized it only for the beam propagated at zero angle. A phase layer with a spherical wavefront is used as an ideal lens. The new design of a Fourier conjugate AO

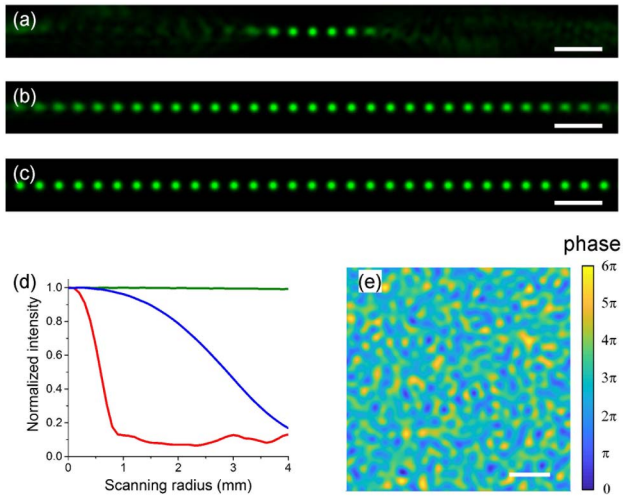

Fig. 3. (a)–(d) Results of simulated beam profiles on the output for different input angles using a beam propagation method. (a)–(c) Sums over simulated focal points distributed with a step of 0.2 mm for (a) the standard conjugate AO approach, (b) the first configuration of Fourier conjugate AO approach, (c) the second configuration of Fourier conjugate AO approach. (d) Normalized peak intensity as a function of scanning radius for standard conjugate AO [red line, experimental setup depicted in Fig. 1(a)]; the first configuration of Fourier conjugate AO [blue line, experimental setup depicted in Fig. 1(b)]; and the second configuration of Fourier conjugate AO [green line, experimental setup depicted in Fig. 1(c)]. (e) A single scattering layer used as a random phase mask. Scale bars are (a)–(c) 0.5 mm and (e) 1 mm.

microscope may require a special microscope objective optimized for working in the non-$4f$ imaging system. The following parameters were used to simulate all AO methods [the intersection of blue and red dashed line areas in Fig. 2(b)]: focal lengths $f_1 = f_2 = f_3 = 100$ mm, which lead to $p = 1$, Gaussian beam with input beam diameter $D = 1$ mm and $\lambda = 900$ nm, position of scattering layer (imaging depth) $l = 80$ mm, deep-tissue imaging, $l/f_3 = 0.8$.

The results of simulations are presented in Fig. 3(a) for a standard conjugate AO approach and in Figs. 3(b) and 3(c) for Fourier conjugate AO approaches. I simulate output beam profiles for different input angles and present sum over focal points distributed with a 0.2 mm step. Figure 3(d) shows normalized peak intensity as a function of scanning radius for standard conjugate AO (red line), the first design (blue line), and the second design (green line) of Fourier conjugate AO.

We see that, for standard conjugate AO, the quality of the focal spot degrades fast, as predicted by the analytical model. Theoretical predictions state that the FOV $= 0.8D$ for standard conjugate AO and FOV $= 4D$ for the first configuration of Fourier conjugate AO for chosen parameters of a system. Our simulations show that, at radius $r = 0.4D = 0.4$ mm from the center, the peak intensity decreases to ∼80% of the maximum as well as the quality of focal spot noticeably degrading [see Fig. 3(a)] for the standard conjugate AO approach.

The peak intensity and shape of the focal spot maintained high quality for $r = 0.4$ mm in the case of Fourier conjugate AO. The peak intensity decreases to ∼80% of the maximum,

while the quality of the focal spot noticeably degrades [see Fig. 3(b)] for Fourier conjugate AO approach only at a distance $2D = 2$ mm from the center, as predicted by the theory above. We also see that the FOV for the second configuration of Fourier conjugate AO is not limited because we consider a single scattering layer with an infinite memory effect range.

Advantages of Fourier conjugate AO are achieved by sacrificing microscope telecentricity, as shown in Fig. 1. Loss of telecentricity raises the question about the aberration of the system itself. In order to analyze the properties of the newly designed optical system alone, a ray-tracing tool (i.e., Zemax OpticStudio 17) is used.

A telecentric optical system designed for conventional AO [presented in Fig. 1(a)] and nontelecentric optical system designed for Fourier conjugate AO [presented in Fig. 1(b)] are simulated in Zemax OpticStudio using the same parameters, except for the distance between the last two lenses. Standard achromatic doublet lenses [Thorlabs AC508-100-B-ML] with a focal length of 100 mm are used. Beam diameter is chosen as 10 mm to provide some moderate aberrations. A scan angle of 2.3° corresponds to a scanning radius of 4 mm. Position of the imaging plane is optimized by Zemax for 0° and 2.3° angles, separately.

Results of ray-tracing simulations for the conventional telecentric system are presented in Figs. 4(a)–4(d) and for the proposed nontelecentric system in Figs. 4(e)–4(h). The spot diagrams presented in Figs. 4(a) and 4(e) for 0° angle and in Figs. 4(b) and 4(f) for 2.3° angle give an indication of the image of a point object and, as a result, show the combined effect of aberrations experienced in the ray trace through the optical systems. Black circles represent an Airy radius of 11 μm, which indicates the diffraction-limited spot size. For the 0° angle, both designs do not experience any aberrations, i.e., all spots are within the Airy radius. Moderate aberrations come in for the 2.3° angle. Interesting that the nontelecentric system has less aberrations (points are closer to the center, and more points are within the Airy radius) than the telecentric one. This is a result of using the central part of the last lens in a nontelecentric system. Moreover, it also helps to prevent any vignetting effects, which is typically the result of light rays being blocked by the edges of individual lens elements. These simulations also show that scanning distance of the focus is a linear function of the scanning angle for both designs. Image center positions for telecentric and nontelecentric designs are calculated to be 4.009 and 4.005 mm, respectively.

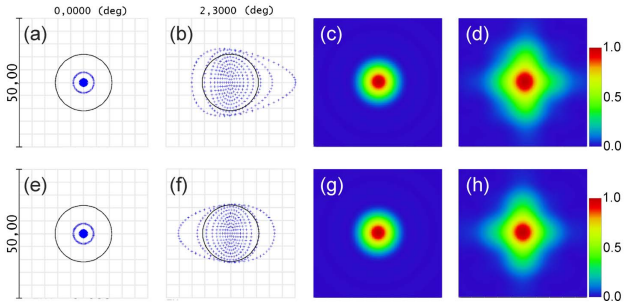

Fig. 4. Simulations of system aberrations in Zemax OpticStudio for (a)–(d) telecentric and (e)–(h) nontelecentric designs. Spot diagrams for (a), (e) 0° angle and for (b), (f) 2.3° angle. Black circles represent an Airy radius of 11 μm, which indicates the diffraction-limited spot size. The Huygens PSF for (c), (g) 0° angle and for (d), (h) 2.3° angle. The loss of telecentricity does not introduce additional aberrations in the focal plane of the system. The scale bars are 50 μm.

In order to analyze point spread function (PSF) behavior, the Huygens PSFs of both optical systems are calculated and presented in Figs. 4(c) and 4(g) for 0° angle and in Figs. 4(d) and 4(h) for 2.3° angle. For each ray, the amplitude, coordinates, direction cosines, and optical path differences are used to compute the complex amplitude of the plane wave incident at every point on the image space grid. A coherent sum for all rays is performed, and the intensity of each point is the square of the resulting complex amplitude sum. Variations of the PSFs across the FOV are similar for standard and nontelecentric designs. As a result, the loss of telecentricity does not introduce additional aberrations of the system.

4. DISCUSSION

Methods of adaptive optics in combination with two-photon microscopy are a promising approach for noninvasive deep-tissue imaging. The proposed technique of Fourier conjugate AO keeps all advantages of well-established conjugate adaptive optics microscopy while providing further improvements, which are especially critical for the case of deep-tissue imaging:

1. It is well known that the position of the SLM in conjugate AO depends on the imaging depth beyond the scattering layer. It can be easily seen from the theoretical analysis presented in the paper that the conventional microscope design of standard conjugate AO is not suitable for imaging far beyond the scattering layer. The theoretically possible imaging depth of standard conjugate AO is limited by the available positions of the SLM. In contrast, Fourier conjugate AO approaches provide imaging depth limited only by working distance of the objective and not by the microscope design itself.
2. The proposed Fourier conjugate AO does not require putting the SLM in the focusing beam. It excludes possible thermal damage due to high-powered lasers, which are widely used for deep-tissue nonlinear microscopy [31]. Moreover, it allows optimal use of SLM resolution, which is critical in the case of wavefront shaping in highly scattering samples (the intensity in the focal spot is proportional to the number of segments used for wavefront shaping) [29].
3. Fourier conjugate AO provides a better way to utilize the angular optical memory effect, as shown in the manuscript. Optimal usage of the optical memory effect will allow the improvement of FOV compared with standard conjugate AO.

Here, analysis was done for a single scattering layer, but it is straightforward that Fourier conjugate AO will keep all advantages such as larger FOV and the convenient practical setup adapted for high imaging depth also for bulk scattering samples. It was shown that the angular memory effect is not only present behind but also inside scattering layers, and the field of view will be mostly limited by the generalized optical memory effect [32]. The overlapping volume between the initial beam and scanning beam in both cases of Fourier conjugate AO are significantly bigger than the overlapping volume in the case of standard conjugate AO, as can be easily seen by comparing

the dark red areas after lens L_3 in Fig. 1(a) and in Figs. 1(b) and 1(c).

To summarize, I proposed and analyzed a powerful method of adaptive optics: Fourier image plane conjugate adaptive optics. The new method provides a higher field of view, which is limited only by the optical memory effect even if precompensation was done for a single point, is more appropriate for deep-tissue imaging, is easier and more stable in experimental implementation, and allows optimal usage of SLM resolution. Advantages of two different experimental configurations of Fourier conjugate AO were demonstrated. The new method can be used as a powerful tool for noninvasive deep tissue optical microscopy.

Funding. Nederlandse Organisatie voor Wetenschappelijk Onderzoek (NWO) (VENI 15872).

Acknowledgment. I thank Ivo Vellekoop and Gerwin Osnabrugge for support and discussions.

REFERENCES

1. D. J. Stephens, "Light microscopy techniques for live cell imaging," Science **300**, 82–86 (2003).
2. B. A. Wilt, L. D. Burns, E. T. Wei Ho, K. K. Ghosh, E. A. Mukamel, and M. J. Schnitzer, "Advances in light microscopy for neuroscience," Annu. Rev. Neurosci. **32**, 435–506 (2009).
3. L. V. Doronina-Amitonova, I. V. Fedotov, A. B. Fedotov, K. V. Anokhin, and A. M. Zheltikov, "Neurophotonics: optical methods to study and control the brain," Phys. Usp. **58**, 345–364 (2015).
4. V. Ntziachristos, "Going deeper than microscopy: the optical imaging frontier in biology," Nat. Methods **7**, 603–614 (2010).
5. F. Helmchen and W. Denk, "Deep tissue two-photon microscopy," Nat. Methods **2**, 932–940 (2005).
6. N. G. Horton, K. Wang, D. Kobat, C. G. Clark, F. W. Wise, C. B. Schaffer, and C. Xu, "In vivo three-photon microscopy of subcortical structures within an intact mouse brain," Nat. Photonics **7**, 205–209 (2013).
7. B. A. Flusberg, E. D. Cocker, W. Piyawattanametha, J. C. Jung, E. L. M. Cheung, and M. J. Schnitzer, "Fiber-optic fluorescence imaging," Nat. Methods **2**, 941–950 (2005).
8. L. V. Doronina-Amitonova, I. V. Fedotov, O. I. Ivashkina, M. A. Zots, A. B. Fedotov, K. V. Anokhin, and A. M. Zheltikov, "Implantable fiber-optic interface for parallel multisite long-term optical dynamic brain interrogation in freely moving mice," Sci. Rep. **3**, 3265 (2013).
9. S. Gigan, "Optical microscopy aims deep," Nat. Photonics **11**, 14–16 (2017).
10. N. Ji, "Adaptive optical fluorescence microscopy," Nat. Methods **14**, 374–380 (2017).
11. M. J. Booth, "Adaptive optical microscopy: the ongoing quest for a perfect image," Light Sci. Appl. **3**, e165 (2014).
12. I. M. Vellekoop and A. P. Mosk, "Focusing coherent light through opaque strongly scattering media," Opt. Lett. **32**, 2309–2311 (2007).
13. I. M. Vellekoop, A. Lagendijk, and A. P. Mosk, "Exploiting disorder for perfect focusing," Nat. Photonics **4**, 320–322 (2010).
14. S. Rotter and S. Gigan, "Light fields in complex media: mesoscopic scattering meets wave control," Rev. Mod. Phys. **89**, 015005 (2017).
15. J. M. Girkin, S. Poland, and A. J. Wright, "Adaptive optics for deeper imaging of biological samples," Curr. Opin. Biotechnol. **20**, 106–110 (2009).
16. T. Wu and M. Cui, "Numerical study of multi-conjugate large area wavefront correction for deep tissue microscopy," Opt. Express **23**, 7463–7470 (2015).
17. L. Kong and M. Cui, "In vivo deep tissue imaging via iterative multiphoton adaptive compensation technique," IEEE J. Sel. Top. Quantum Electron. **22**, 40–49 (2016).
18. R. K. Tyson, *Principles of Adaptive Optics* (CRC Press, 2015).
19. J.-H. Park, L. Kong, Y. Zhou, and M. Cui, "Large-field-of-view imaging by multi-pupil adaptive optics," Nat. Methods **14**, 581–583 (2017).
20. I. Freund, M. Rosenbluh, and S. Feng, "Memory effects in propagation of optical waves through disordered media," Phys. Rev. Lett. **61**, 2328–2331 (1988).
21. S. Feng, C. Kane, P. A. Lee, and A. D. Stone, "Correlations and fluctuations of coherent wave transmission through disordered media," Phys. Rev. Lett. **61**, 834–837 (1988).
22. J. Mertz, H. Paudel, and T. G. Bifano, "Field of view advantage of conjugate adaptive optics in microscopy applications," Appl. Opt. **54**, 3498–3506 (2015).
23. L. Amitonova, G. Osnabrugge, T. Knop, and I. Vellekoop, "Variable-conjugation plane adaptive optics microscope for deep-tissue bioimaging," Proc. SPIE **10502**, 105020H (2018).
24. J. Li, D. R. Beaulieu, H. Paudel, R. Barankov, T. G. Bifano, and J. Mertz, "Conjugate adaptive optics in widefield microscopy with an extended-source wavefront sensor," Optica **2**, 682–688 (2015).
25. H. P. Paudel, J. Taranto, J. Mertz, and T. Bifano, "Axial range of conjugate adaptive optics in two-photon microscopy," Opt. Express **23**, 20849–20857 (2015).
26. J. Li, T. G. Bifano, and J. Mertz, "Widefield fluorescence microscopy with sensor-based conjugate adaptive optics using oblique back illumination," J. Biomed. Opt. **21**, 121504 (2016).
27. X. Tao, T. Lam, B. Zhu, Q. Li, M. R. Reinig, and J. Kubby, "Three-dimensional focusing through scattering media using conjugate adaptive optics with remote focusing (CAORF)," Opt. Express **25**, 10368–10383 (2017).
28. J.-H. Park, W. Sun, and M. Cui, "High-resolution in vivo imaging of mouse brain through the intact skull," Proc. Natl. Acad. Sci. USA **112**, 9236–9241 (2015).
29. I. M. Vellekoop and A. P. Mosk, "Phase control algorithms for focusing light through turbid media," Opt. Commun. **281**, 3071–3080 (2008).
30. O. Katz, E. Small, Y. Guan, and Y. Silberberg, "Noninvasive nonlinear focusing and imaging through strongly scattering turbid layers," Optica **1**, 170–174 (2014).
31. P. Theer, M. T. Hasan, and W. Denk, "Two-photon imaging to a depth of 1000 μm in living brains by use of a Ti: Al2O3 regenerative amplifier," Opt. Lett. **28**, 1022–1024 (2003).
32. G. Osnabrugge, R. Horstmeyer, I. N. Papadopoulos, B. Judkewitz, and I. M. Vellekoop, "Generalized optical memory effect," Optica **4**, 886–892 (2017).